Environ. Sci. Technol. 1994, 28, 63–72

Desorption of Halogenated Organics from Model Solids, Sediments, and Soil under Unsaturated Conditions. 2. Kinetics

James Farrell[†] **and Martin Reinhard***

Department of Civil Engineering, Stanford University, Stanford, California 94305

The mechanisms controlling desorption rates from soils and sediments were investigated by measuring TCE desorption kinetics from model solids, sediments, and soil under unsaturated conditions at 100% relative humidity. A new experimental methodology enabled measurement of desorption rates over more than 7 orders of magnitude and revealed that intraparticle pores of molecular dimensions may be responsible for the slow release of sorbed contaminants. Desorption kinetics proceeded on two distinct time scales, and all solids had both a fast and slowly released fraction. The amount of slow desorbing TCE was found to depend on the initial vapor concentration, but not in direct proportion. At TCE vapor concentrations near saturation, the fast fraction comprised the majority of the sorbed TCE and required less than 10 min for desorption, whereas the slow desorbing fraction was released over periods of months to years. Although model solids with uniform pore and particle sizes were used, a pore diffusion model was not adequate to describe both the fast and slow desorbing fractions. The measured physical properties of the solids were not useful for making *a priori* predictions and, in comparisons among the solids, did not correlate with the amount and the rate of slowly released TCE. The Freundlich isotherm exponents correlated with the fraction of slowly released TCE, but isotherm nonlinearity was not sufficient to account for the dual rate behavior.

Introduction

The kinetics of adsorption and desorption are among the most influential processes affecting the transport and the fate of contaminants in the environment. Furthermore, the slow release of sorbed contaminants is the primary obstacle to remediation of soil and groundwater pollution by pump-and-treat and soil vapor extraction. Investigation of the mechanisms responsible for slow sorption processes have been confounded by the complexities and heterogeneities of natural systems. Studies have implicated both restricted diffusion through soil organic matter (*1*) and restricted diffusion through intraaggregate pores (*2, 3*) as responsible for the persistence of contaminants in the environment. The object of this research was to investigate the mechanisms responsible for slow desorption using both model solids with controlled properties and natural soil and sediments.

Previous studies using batch systems to measure adsorption and desorption kinetics were not able to adequately resolve early time adsorption or desorption because of their inability to provide continuous measurements (*2, 4, 5*). Other investigations—including column studies—capable of continuous measurement lacked adequate resolution for measuring very low rates of uptake or release (*1, 6*). These shortcomings in prior studies have obscured mechanisms and led to conclusions which may not have been supported had the entire spectrum of desorption rates been investigated. The methods used in this study allowed continuous measurement of desorption rates over more than 7 orders of magnitude. The improved methodology was used to measure desorption kinetics for trichloroethylene (TCE) from six model solids, two aquifer materials, and one soil.

Theory

Pore Diffusion Model. Even under conditions representative of the vadose zone, capillary condensation leads to the internal pores of soil particles and aggregates being water-filled. Therefore, in both the saturated and the unsaturated zones, desorption of contaminants bound within soil particles requires diffusion through water-filled pores. The pore diffusion model provides a framework for understanding solute mass transfer within porous particles and aggregates. A mathematical description of diffusional mass transfer requires an assumption of the particle or aggregate geometry. If the particles are approximated as spheres, Fick's second law of diffusion within the particle can be expressed as (*7*)

$$\frac{\delta C_w}{\delta t} = \frac{D_e}{r^2}\frac{\delta}{\delta r}\left(r^2\frac{\delta C_w}{\delta r}\right) \tag{1}$$

The notation for eq 1 and all subsequent equations is given in the glossary following the text. Equation 1 describes the concentration of adsorbate as a function of time and position within the immobile fluid which fills the internal pores of a soil particle or aggregate. As eq 1 is written, the driving force for diffusion is the concentration gradient in the aqueous phase, surface diffusion is ignored, and diffusion occurs only through the aqueous phase.

The effective diffusion coefficient, D_e, reflects the rate at which the solute appears to diffuse through the particle. It accounts for the fraction of the time that the diffusing species is adsorbed on the solid surface and is therefore immobile. The actual rate at which the solute diffuses through the pore fluid is represented by the pore diffusion coefficient, D_p. For linear partitioning, D_p is related to D_e by the expression:

$$D_e = \frac{D_p}{\left[1 + \frac{\rho_g}{\epsilon_i}K_d\right]} \tag{2}$$

The denominator in eq 2 is referred to as the internal retardation factor, R_{int} (*2*). R_{int} is the ratio of the diffusion rate of an adsorbing species to that of a nonadsorbing solute with the same pore diffusivity. Equation 2 assumes a linear adsorption isotherm and shows that the rate of diffusive uptake or release decreases with increasing isotherm slope, K_d.

[†] Present address: Failure Analysis Associates, 149 Commonwealth Dr., Menlo Park, CA 94025.

0013-936X/94/0928-0063$04.50/0

If the adsorption isotherm is nonlinear, D_e is dependent on the solute concentration within the particle. If the Freundlich isotherm model is used to represent the nonlinear sorption isotherm, D_e can be expressed as

$$D_e = \frac{D_p}{1 + \frac{\rho_g}{\epsilon_i}\left[K_F \frac{1}{n} C_w^{(1/n-1)}\right]} \quad (3)$$

For solids with $1/n < 1$, the bracketed term in the denominator of eq 3 increases with decreasing sorbate concentration, thereby decreasing D_e.

Because pore diffusion occurs through the aqueous phase, the rate of pore diffusion can be related to the aqueous diffusivity of the adsorbate if the effects of tortuous paths and steric hindrance are taken into account. Steric hindrance results from pore constrictions and pore walls shortening the mean-free-path of the diffusing molecules. Steric hindrance increases with decreasing pore size and becomes very large as pore size approaches molecular dimensions (*8*). Tortuous and dead-end pores lead to longer diffusional paths to travel a given radial distance within a particle or aggregate. Both steric hindrance and tortuosity serve to reduce the pore diffusivity of the solute to a fraction of its aqueous diffusivity. An expression which accounts for these two effects has been proposed by Satterfield et al. (*9*) to relate the bulk aqueous diffusion coefficient, D_a, and D_p by

$$D_p = \frac{K_r}{\chi} D_a \quad (4)$$

The restrictivity factor, K_r, accounts for steric hindrance in small pores, and the tortuosity factor, χ, accounts for the increased path length for a given radial distance. The restrictivity factor is a function of both the solute and pore sizes and has been found to correlate with their ratio, λ, as given by (*8*)

$$K_r = 1.03 \exp(-4.5\lambda) \quad (5)$$

Wakao and Smith (*10*) found the tortuosity factor for diffusion through porous catalysts to be inversely related to the porosity of the particle and can be estimated by

$$\chi = 1/\epsilon_i \quad (6)$$

Since K_r and χ are only approximate representations of real phenomena and cannot be independently determined, they are often grouped into an effective tortuosity, χ_e, as given by

$$\chi_e = \chi/K_r \quad (7)$$

Based on the measured isotherm parameters and the physical properties of the solid, eqs 2–6 can be used to estimate an *a priori* effective diffusion coefficient for any solute and sorbent pair.

Limitations of Pore Diffusion Model. A serious limitation of the pore diffusion model is the assumption that the distribution of pores can be characterized by a representative, average D_e. Implicit in this assumption is that there exists a continuum in properties and behavior across the entire pore size spectrum. This continuum assumption, however, breaks down as pore diameters approach molecular dimensions.

Because pore size can influence both the amount and kinetics of adsorption, pores have been classified according to size (*11*). Cylindrical pores with diameters <20 Å or slit-shaped pores of this width are classified as micropores. Pores with diameters between 20 and 500 Å are classified as mesopores, while pores >500 Å are classified as macropores. The dividing diameters are not firm, but each class of pores is associated with a characteristic adsorptive behavior. Capillary condensation is associated with mesoporosity, while solids possessing only macroporosity show little or no capillary effects (*12*). Because micropores are of molecular dimensions, several additional factors govern sorption in these pores.

Molecules adsorbed in micropores are subject to stronger field strengths than those adsorbed on flat surfaces (*13*). Adsorption energies are substantially increased because of the superposition of interaction potentials of opposing walls. Higher adsorption energies lead to increased adsorption and, as presented in the preceding article (*14*), contribute to isotherm nonlinearity for sorbents with pores less than several adsorbate diameters in size.

In micropores, increased sorption leads to reduced diffusive transport rates through the effect of isotherm slope on R_{int}. Aside from increased adsorption, there are two additional contributions to reduced transport rates in micropores. The first contribution is that steric hindrance increases exponentially as the pore size approaches the size of the solute (*8*). The second contributing factor is that as pore size decreases, the ratio of pore surface area to pore volume increases. Even if the K_d remains the same, the ratio of adsorbate mass on the surface to adsorbate mass in solution is greater in smaller pores. The result is that a given adsorbate molecule spends relatively more time adsorbed on the surface than in solution for smaller pores compared to larger pores. If diffusion occurs only through the solution phase, the D_e is reduced in smaller pores because the adsorbate spends less time diffusing. Even in the presence of surface diffusion, transport rates are still reduced because of the relative slowness of surface diffusion compared to aqueous diffusion (*15*). Therefore, even for a constant partitioning coefficient, smaller pores lead to higher internal retardation.

In light of these factors, assuming homogeneity among the pores can be a significant oversimplification for microporous sorbents. Sorbent microporosity leads to three effects: increased steric hindrance, increased sorption energies, and greatly increased surface area to volume ratios, all of which contribute to reduce desorption rates.

Although a number of researchers have found success in applying the pore diffusion model to the uptake and the release of organic contaminants (*2, 6*), the fits may be based on an inappropriate physical model. A major shortfall in previous investigations is that adsorption or desorption rates were measured over limited concentration ranges. Mechanisms—such as sorption in micropores—that may be dominant at one concentration range but contribute only marginally at another may be obscured in investigations covering limited concentration ranges. Wu and Gschwend (*6*) found that the pore diffusion model was adequate to describe both adsorption and desorption kinetics for several nonpolar organic sorbates on soils and sediments. However, the range of concentrations investigated was less than 2 orders of magnitude, and the resolution of slow phenomena was not possible. Where the range of experimental data is limited, mechanisms may be overlooked although models may fit the data. However, these models may lead to erroneous conclusions since they may not be applicable if extrapolated beyond

the range for which the parameters were determined. Data from this study indicate that, for limited concentration ranges, fits can be made with the pore diffusion model, but the best fit parameters for a given sorbent are concentration dependent and, are therefore, not mechanistically representative of the true phenomena.

Ball and Roberts (2) found that a pore diffusion model fit data for PCE uptake on Borden sand if an instantaneously adsorbed fraction was assumed. Assuming an instantaneously adsorbed fraction is an *a priori* limit on the concentration range investigated and provides a second fitting parameter—both of which obscure the early time mechanisms for sorptive uptake.

In order to obtain meaningful physical parameters, the length scale over which the characteristic D_e applies must be the particle radius. If this is not the case, the pore diffusion model defaults to a nonmechanistic model with a fitting parameter, χ_e. Nonmechanistic bases for fits to the pore diffusion model may explain inconsistent observations on the effects of particle size on adsorption rates. Ball and Roberts (2) found that pulverization of their adsorbent particles increased adsorption rates, but the increase was less than expected based on pore diffusion parameters derived from the original material. Additionally, Steinberg et al. (*16*) observed that pulverization greatly increased desorption rates of ethylene dibromide (EDB) from two soils, but for the original material, rates of release were only weakly dependent on particle size. Therefore, although the pore diffusion model may fit experimental data, if the underlying physical mechanisms do not correspond to the model formulation, the model will not be useful for predictive purposes under different circumstances.

Experimental Section

The procedures and equipment used for measuring the desorption isotherms described in the preceding paper (*14*) were used for measuring the TCE desorption kinetics. Stainless steel columns (25 cm × 9 mm i.d.) containing one of the sorbents contaminated with TCE were purged with a stream of nitrogen humidified at 100% relative humidity. The effluent TCE was measured with flame ionization detector (FID) mounted on a Hewlett Packard (HP) 5890 gas chromatograph (GC). To measure desorption rates below the detection limit of the FID, the sorbent column effluent was trapped on a column of Tenax (Alltech) polymer beads for periods ranging from 3 min to 1 h. The Tenax polymer was then thermally desorbed on a Tekmar dynamic headspace concentrator and analyzed on an HP GC equipped with a Hall detector. The length of the Tenax trapping period was increased as required to measure the decreasing TCE desorption rates. After purging the TCE contaminated sorbents for periods ranging from 1 week to 1 month, the columns were heated to remove the residual TCE remaining on the solids. Full details of the experimental procedures are contained in ref 17. The physical properties of the solids and desorption isotherms for TCE on these solids are given in the preceding paper (*14*).

To assure that sorptive equilibrium was achieved in the columns prior to purging, identical experiments were performed with different equilibration periods. Increasing the equilibration periods from 1 to 3 months resulted in no measurable differences in experimental outcomes. Therefore, if equilibrium is not reached within 1 month, the required equilibration periods must greatly exceed 3 months. Since equilibration periods greatly exceeding 3 months have not been observed for low molecular weight, low-sorbing compounds, all columns prior to purging were most assuredly at equilibrium.

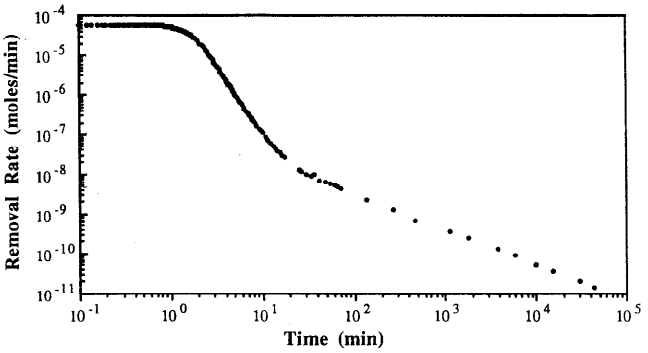

Figure 1. Rate of TCE desorption from a column containing 5.9 g (dry wt) of silica A with an initial TCE vapor saturation of 79% P/P_0 purged at 15 mL/min.

Results and Discussion—Model Solids

The model solids used in this study were chosen to investigate the effects of pore size, particle size, and lack of internal porosity on desorption kinetics. Desorption experiments were performed on four silica gels of varying pore size and particle size, glass beads, and on the clay mineral montmorillonite. The silica gels possess both meso- and microporosity while the glass beads possess only microporosity. The montmorillonite was used as a model for nonporous solids.

Meso- and Microporous Solids. A 4-week (4×10^4 min) TCE removal rate profile for silica A is shown in Figure 1. The purge flow rate for all kinetic experiments ranged between 15 and 18 mL/min, corresponding to 2–3 pore vols/min and ~0.75 cm/s linear velocity. The TCE removal rate profiles on all solids were characterized by three desorption regimes which can be seen in Figure 1. The first desorption regime occurs during the initial ~2 min of purging where the effluent vapor concentration remains nearly constant although ~5 pore vol have been eluted. This indicates fast desorption is occurring and that column effects are influencing the TCE removal rate. Column effects include axial dispersion and repeated cycles of adsorption and desorption as a TCE molecules traverses the length of the column. While purging the first 5 pore vols, column effects contributed to a desorption front of nearly constant concentration traveling through the column.

During the first desorption regime, the TCE removal rate is proportional to the purge flow rate. A second desorption regime occurs between ~2 and 10 min elapsed where the TCE removal rate is dependent on the purge rate, but is not directly proportional. The third desorption regime occurs after ~10 min where the rate of TCE removal is independent of the purge rate, for the range in rates investigated (0.25–4 pore vols/min). These three desorption regimes were observed on all solids, and independence of the removal rate with the purge rate occurred within ~10 min in all cases. At this time, mass transfer limitations within the sorbent particles were controlling the rates of TCE removal, and the vapor phase mass transfer resistance was negligible. After ~20 min had elapsed, the effluent sorbate vapor concentrations

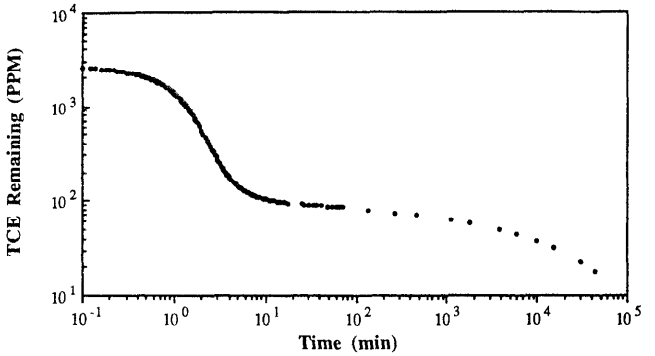

Figure 2. TCE remaining in ppm (dry weight of solids) for the silica A column in Figure 1.

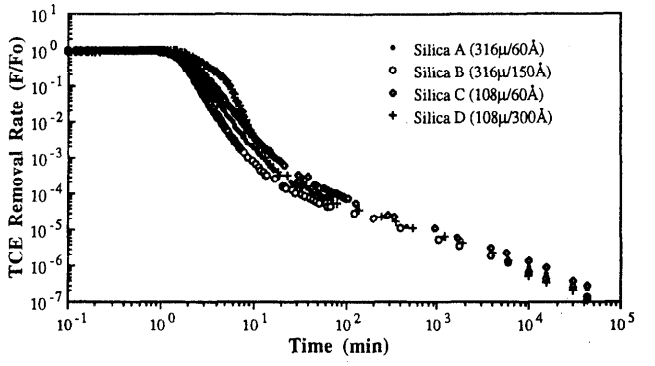

Figure 3. Rate of TCE removal normalized to the initial rate for columns of four silica gels of different pore and particle size with initial TCE vapor saturations of 79% P/P_o purged at 15 mL/min.

were 2–5 orders of magnitude below the equilibrium vapor concentrations. Experiments with a nonsorbing tracer (5% methane in argon) confirmed the absence of unswept zones in the columns.

From a removal rate profile and the residual sorbed TCE recovered by thermal desorption after purging, the mass of TCE in the column as a function of time can be determined. Figure 2 shows the TCE remaining as a function of time for the Silica A removal rate profile in Figure 1. The sharp bend in the curve at 6 min corresponds to the point where the removal rate becomes flow rate independent.

Pore and Particle Size. Four silica gels with monodisperse particle sizes and narrow pore size distributions were used to investigate the effects of pore and particle size on desorption kinetics. Figure 3 compares the TCE removal rates [the removal rate from each column (in mol/min) is normalized by the initial removal rate], and Figure 4 compares the TCE remaining on the four silicas whose properties are summarized in Table 1. The initial vapor concentrations were the same in each column and were equal to ~79% P/P_o TCE saturation. This high vapor saturation resulted in capillary condensation of TCE in the silica D column because the internal pores of the silica were not completely water-filled. The silica D water loading of 1.59 mL/g was insufficient to completely fill the pores which have a capacity of 1.70 mL/g. Capillary condensation, therefore, accounts for the silica D column having twice the initial amount of TCE as the other silicas in Figure 4.

Figures 3 and 4 show that both the normalized removal rate and the TCE remaining profiles for the four silicas are similar in shape. Figure 4 indicates that there are two distinct time scales for desorption. Over 95% of the

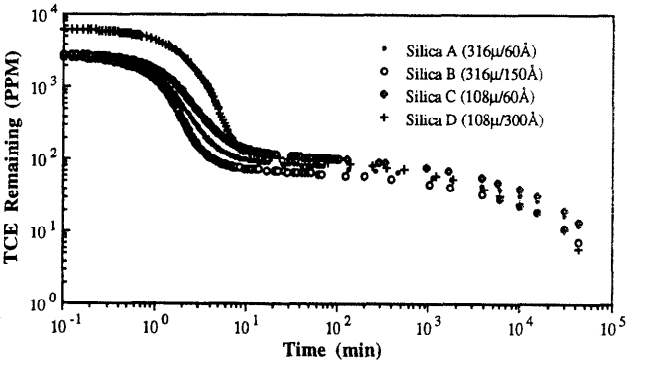

Figure 4. TCE remaining on four silica gels for the removal rate profiles in Figure 3.

Table 1. Physical Properties, Freundlich Isotherm Exponents for Aqueous Adsorption, and Residual TCE for Four Silica Gels in Figures 3 and 4

silica	surface area (m^2/g)	pore diameter (Å)	particle diameter (μm)	Freundlich exponent	residual TCE (ppm)
A	297	60	316	0.61	12
B	267	150	316	0.64	8.2
C	394	60	108	0.55	14
D	242	300	108	0.71	6.1

initially sorbed TCE is released during the first 10 min; however, the remaining TCE desorbs on a time scale of months.

On the basis of the pore diffusion model, particle size differences between silicas A and C should lead to faster desorption from silica C. In the pore diffusion model, the dimensionless time scale for radial diffusion, τ_d, is inversely proportional to the square of the particle radius as given by (7)

$$\tau_d = \frac{D_e t}{r_a^2} \tag{8}$$

Based on the ratio of particle radii, the dimensionless time scale for silica A is 8.5 times that of silica C; i.e., to achieve a given level of TCE removal, silica A should require 8.5 times longer than silica C. Figures 3 and 4 contradict this expectation based on the pore diffusion model and show that both the measured removal rate and the mass remaining profiles for silicas A and C are nearly identical. Therefore, if pore diffusion is controlling the slowly released fraction, the length scale for the slow diffusion is not the particle radius. Because these silica gels contain no organic matter, the slow desorption after 10 min cannot be attributed to restricted diffusion through natural organic matter, as suggested in previous investigations with natural materials (*1, 18, 19*).

The effect of pore size on desorption kinetics can be seen in comparisons between silicas A and B, and in comparisons between silicas C and D. The relationship between pore size and steric hindrance given by eq 5 indicates that smaller pores lead to more restricted diffusion. For these silicas, the smaller pore diameters also lead to lower internal porosities, which according to eq 6, should result in higher tortuosities. Table 2 compares the effects of pore size and internal porosity on the calculated *a priori* χ_e for the four silicas. Combining the effects of R_{int} along with calculated χ_e (from eqs 5–7) leads to the *a priori* D_e given in the last column of Table 2.

Table 2. Comparison of Calculated R_{int} and *a Priori* Estimates of Mass Transfer Parameters for Four Silica Gels

silica	R_{int}[a]	χ	K_r	χ_e	D_e/D_a
A	2.48	1.6	0.64	2.5	0.16
B	1.76	1.4	0.85	1.6	0.34
C	2.60	1.6	0.64	2.5	0.15
D	1.23	1.3	0.94	1.4	0.59

[a] Based on initial solids concentration.

Table 3. Variation in R_{int} with Sorbed Concentration for Silica A

time (min)	concn sorbed (ppm)	C_s/C_w (mL/g)	R_{int} (–)
1	2000	0.60	1.8
100	77	3.7	5.9
10000	32	6.0	9.0
40000	12	11	15

Based on differences in D_e, silica B should have desorption kinetics which are twice as fast as silica A; and desorption kinetics for silica D should be four times faster than those for silica C. However, Figures 3 and 4 show that the data do not follow pore diffusion model expectations based on the internal porosities and pore diameters.

The effect of isotherm nonlinearity on R_{int} is illustrated in Table 3. Using the measured Freundlich parameters, estimates for R_{int} based on the sorbed concentrations can be made. For silica A, Table 3 shows that D_e decreases with TCE removal. Because of isotherm nonlinearity, R_{int} increases by a factor of 8 over the course of the experiment. However, since the increase in R_{int} is less than a factor of 3 between 1 and 10 min, an increased R_{int} is insufficient to account for the greatly decreased desorption rates occurring after 10 min.

Numerical Simulations. A numerical simulation of the pore diffusion model has been developed and utilized by Grathwohl and Reinhard (*20*). The required model inputs are the diameters, densities, and porosities of the particles, the isotherm parameters, the initial adsorbate concentration; and χ_e—the only fitting parameter. The model assumes a uniform initial solute distribution within the particle and a zero concentration external to the particle for times >0. A caveat in applying this model to the experimental data is that during the first several min of purging, the experimental conditions differ from the model formulation in that the TCE concentration external to the particles is not zero. Only at the inlet of the column is the TCE vapor concentration zero, and column effects during the first several min influence the TCE concentration external to the sorbent particles. However, differences between the experimental conditions and the model formulation become negligible several min into the experiment after the TCE removal rate becomes flow rate independent.

Figure 5 compares the mass remaining profiles for three numerical simulations with the experimental data for silica A. The model simulations demonstrate the effects of isotherm shape and χ_e on TCE desorption kinetics. The numerical simulation based on the *a priori* estimated χ_e is given by profile A in Figure 5. Except for the slowly released fraction, the simulation profile and the experimental data are similar in shape. Displacement of the experimental data from the simulation profile, in part, results from column effects and the disparity between the

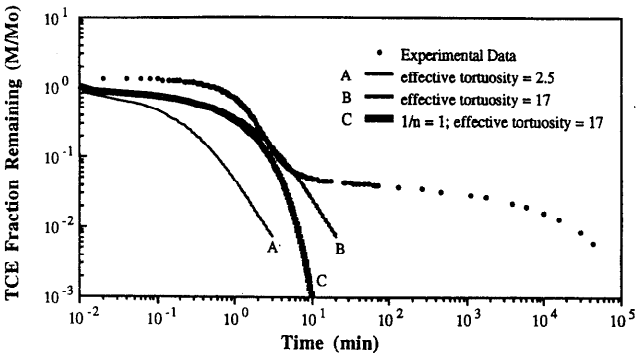

Figure 5. Comparison of model simulations and experimental data for the silica A TCE desorption data in Figures 1–4.

model formulation and experimental conditions. For the experimental data, the mass remaining in the column is normalized by the initially sorbed TCE and ignores TCE in the column void space prior to purging. This accounts for $M/M_o > 1$ during the first half minute of the experimental data.

If χ_e is increased to better fit the experimental data, as in profile B of Figure 5, the maximum overlap of the simulation profile and the experimental data occurs for $\chi_e = 17$. Because the early time disparity between the model formulation and the experimental conditions serves to reduce the measured desorption rates relative to the model, the actual best fit χ_e is between 2.5 and 17. A comparison of profiles A and B in Figure 5 shows that the effect of increasing χ_e is to displace the simulation profile along the time axis while maintaining the same shape. Based on the measured physical and isotherm properties for silica A, the pore diffusion model cannot represent both the initial fast desorption and the secondary slow release which occurs after 10 min. Curve C in Figure 5 shows the effect of isotherm shape on the simulation profiles. A linear fit to the silica A TCE isotherm data was used to calculate the R_{int} in the curve C simulation. The curve C simulation shows that isotherm nonlinearity has little effect on the first 90% of TCE removal, but for fractional removals greater than 90%, isotherm nonlinearity does measurably affect the simulation profile and may significantly increase removal times for high fractional removals.

Simulation profile B and the experimental data both show that the first 95% of TCE desorption occurs on a time scale of several min. However, desorption of the last 5% occurs on a time scale of months and cannot be simulated by the pore diffusion model. Two different phenomena appear to control the rate of TCE desorption. At early times, and for the majority of the sorbed TCE, pore diffusion controls TCE desorption. However, after 10 min, a secondary mechanism is required to explain the small fraction which is slowly released.

Table 1 shows that the amount of residual TCE remaining after 1 month of purging correlates with the surface areas of the silicas and inversely correlates with the Freundlich isotherm exponents. Since microporosity may lead to both isotherm nonlinearity and slow desorption, adsorption in micropores is consistent with the slowly released fraction.

Heat Treatment. Heating silica gels which were produced by condensation from aqueous solution has been shown to increase the silica microporosity (*13, 21*). The high viscosity of the solution from which the gels are

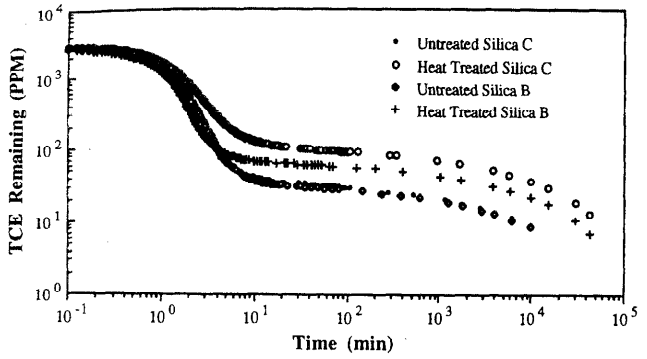

Figure 6. Effect of heat treatment on TCE desorption from columns of silicas B and C.

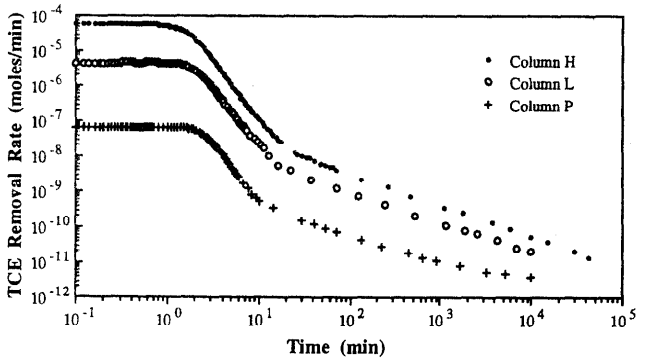

Figure 7. Comparison of TCE removal rates for three columns of silica A purged at ~15 mL/min with initial vapor concentrations of: column H = 3.9×10^{-6} mol/mL; column L = 2.9×10^{-7} mol/mL; and pre-purged column P = 4.0×10^{-9} mol/mL.

condensed leads to steric hindrances and incomplete condensation of neighboring molecules. During the drying process, some of the incompletely condensed poly- and monosilicic acid molecules remain within the structure of the gel. Heating the silica drives off a portion of these molecules and creates pores of molecular dimensions. If microporosity were responsible for the slowly released fraction, heating the silica gels should result in an increase in the amount of slowly released TCE.

Figure 6 compares heat treated (180 °C for 24 h) and untreated columns of silicas B and C. The heat-treated columns of both silicas B and C had significantly higher amounts of slowly released TCE than the untreated columns. This effect was also observed on silica D and supports the contention that microporosity is responsible for the slow desorbing fraction.

Initial Concentration. The effect of initial concentration on TCE desorption kinetics was investigated on silica A. Because of higher adsorption energies, solute preferentially adsorbs in micropores. Since these micropores have a limited sorption capacity, lower initial concentrations may result in a higher fraction of the TCE uptake sorbed in micropores. Therefore, if microporosity is responsible for the slowly released TCE, the fraction of slow desorbing TCE should be greater for lower initial vapor concentrations.

Figure 7 shows that the TCE removal rate profiles for three different initial vapor concentrations on silica A are similar in shape. For columns H and L, the initial TCE vapor concentrations at the start of the purge in Figure 7 were the highest TCE concentrations to which these solids were exposed. Columns H and L were both allowed to equilibrate with the TCE vapor for 1 month prior to

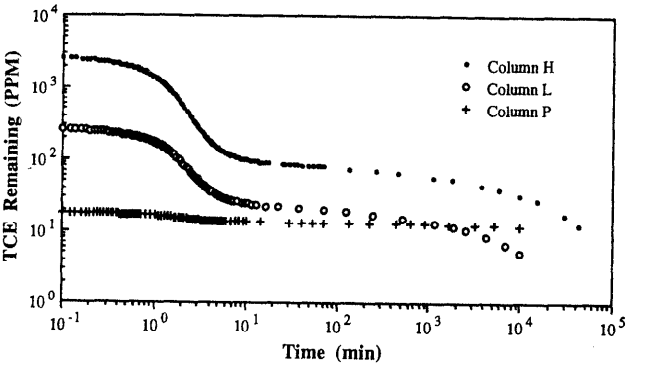

Figure 8. TCE remaining in three columns of silica A with different initial concentrations for the removal rate data in Figure 7.

purging. The solids in column P, however, were purged previously to the purge shown in Figure 7. Column P was initially exposed to the same high TCE concentration as column H, allowed to equilibrate for 1 month, and then purged. After 1 month of purging, column P was sealed and allowed to reequilibrate for 12 weeks before the purge shown in Figure 7 was begun.

Figure 8 shows the amount of TCE remaining as a function of time in each column. Although both the initial vapor concentration and the initial solids concentration in column L were more than 10 times higher than in column P, after purging, column P contained more TCE than column L. The difference in residual TCE between columns L and P can only be explained by hysteresis leading to different distributions of sorbed TCE within the silica particles. Although column P had a lower initial TCE concentration, it had more TCE sorbed in slow sites as compared to column L. The initial TCE distribution between the vapor and sorbed phases in column L represents sorption in the adsorptive direction of the TCE isotherm. For the initial vapor concentration in column L, the sorbed concentration was 30% below the sorbed concentration on the desorption isotherm for that vapor concentration (cf. Figure 3 in ref 14). Since the initial sorbed/vapor distribution in column P is representative of the desorption branch of the TCE isotherm, there appears to be hysteresis between adsorption and desorption on this silica gel.

In addition to hysteresis, Figure 8 also shows that the fraction of sorbed TCE which is slowly released is inversely related to the initial concentration. Because the TCE isotherms on silica A are nonlinear, lower concentrations have a higher R_{int} for pore diffusion. Therefore, isotherm nonlinearity may account for some of the differences in the fractional TCE removals between columns H, L, and P. However, the effect that differences in R_{int} have on the model simulations for columns L and P in Figure 9 is less than differences in the experimental data between columns L and P. If the χ_e which matches the column H data ($\chi_e = 17$) is used to model column L, the simulation gives a similar time as the experimental data for release of 90% of the sorbed TCE. However, a simulation for column P using this same χ_e ($\chi_e = 17$) underestimates the time for 90% TCE removal by several orders of magnitude.

The pore diffusion model with a $\chi_e = 17$ is reasonably able to describe desorption of 95% of the sorbed TCE from column H, and 90% from column L. The similar model and experimental times for 90–95% TCE desorption from columns H and L are an indication that pore diffusion controls desorption from the fast sites. In column P,

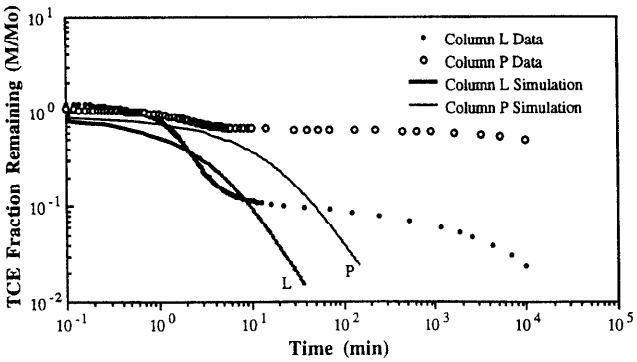

Figure 9. Comparison of simulations with experimental data for columns L and P of silica A for the data in Figures 7 and 8.

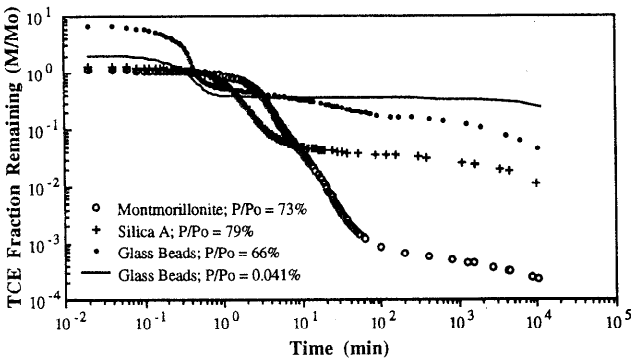

Figure 10. Fraction of initially sorbed TCE remaining on microporous glass beads, nonporous montmorillonite, and meso- and microporous silica gel in columns with initial TCE vapor concentrations near saturation. Also shown is a desorption profile from a column of glass beads with a lower initial TCE vapor saturation of P/P_o = 0.041%.

however, nearly all the TCE is sorbed in slow sites, and the pore diffusion model using the χ_e for the fast sites (i.e., the macro- and mesopores) greatly overestimates TCE desorption rates.

Microporous and Nonporous Solids. The clay mineral montmorillonite was used to investigate desorption kinetics on a nonporous solid. Although montmorillonite is an expanding clay mineral, it is effectively nonporous to nonpolar organic sorbates which cannot penetrate the clay interlayers (*22*). Desorption kinetics from microporous glass beads were also investigated. Nitrogen adsorption measurements on the glass beads indicated no mesoporosity. However, a high BET energy parameter for nitrogen adsorption and an excessively high BET surface area (*14*) were strong indications of microporosity (*23*).

Figure 10 compares the TCE desorption kinetics for montmorillonite, silica A, and two initial concentrations on the glass beads. Comparing the montmorillonite, silica A, and high-concentration glass bead profiles shows that the nonporous montmorillonite had the smallest fraction of slowly released TCE, while the microporous glass beads had the highest fraction. The silica gel, which contains both meso- and microporosity, had an intermediate fraction of slowly released TCE.

The fast desorption from the montmorillonite clay primarily results from its lack of internal porosity. The low residual TCE on the montmorillonite is in agreement with studies on EDB desorption by Pignatello (*4, 5*) and Steinberg et al. (*16*), which found that the clay fraction had the lowest desorption residual of any soil fraction. Because the clay had the highest surface area and most

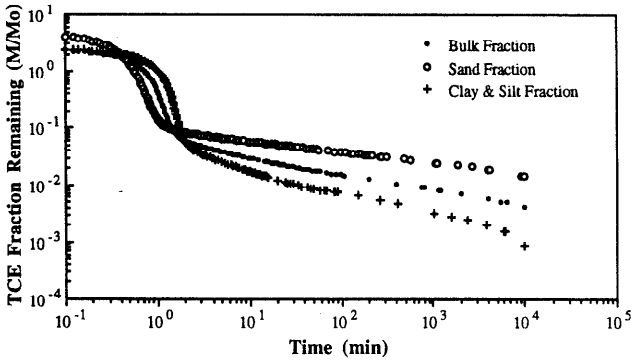

Figure 11. Fractions of initially sorbed TCE remaining for three size fractions of the Livermore Aquifer solids with initial TCE saturations of ~70% P/P_o purged at ~17 mL/min.

Table 4. Freundlich Exponents for Vapor Sorption, Internal Retardation Factors, and Measured Times for 99% TCE Removal on Livermore Size Fractions

size fraction	$1/n$	R_{int}[a]	99% removal time (min)
sand	0.65	1.13	4×10^4
bulk	0.79	1.12	518
clay and silt	1.01	10.1	30

[a] Based on initial solids concentration.

active surface chemistry of all the fractions, Pignatello concluded that high energy sorption on mineral surfaces was not responsible for slow desorption (*5*).

The TCE remaining on the solids in Figure 10 represents the fraction of the total uptake, i.e., both TCE adsorbed on the solid surfaces and TCE partitioned into the adsorbed water layer. Because of the low glass beads surface area, the amount of TCE adsorbed on the surface at the high TCE concentration (P/P_o = 66%) represents only 12% of the total TCE uptake. Since only a small fraction of the total uptake on the glass beads represents adsorption in micropores, a significantly larger fraction of the TCE actually adsorbed on the surface is slowly released than is indicated by the profile in Figure 10. Also shown in Figure 10 is a desorption profile for a lower initial TCE concentration on the glass beads. The lower initial concentration results in a greater slow desorbing fraction compared to the higher initial TCE concentration. This observation can be explained by preferential adsorption on slow sites having a limited sorption capacity.

Results—Natural Solids

Livermore Aquifer Solids. *Size Fractions.* The fractions of initially sorbed TCE remaining on three size fractions of the Livermore Aquifer solids are shown in Figure 11. Table 4 compares the Freundlich isotherm exponents, the initial R_{int}, and the measured times required for 99% TCE removal for the three Livermore size fractions. The times required for 99% TCE removal inversely correlate with the Freundlich exponents. The smaller particle size of the clay and silt fraction may contribute to faster TCE release by shortening the diffusional distances required for desorption. Additionally, the higher external surface area associated with smaller particles may lead to more adsorption on external surfaces, thereby eliminating any pore diffusional limitations.

The effects of isotherm shape on R_{int} cannot account for the shorter 99% TCE removal time for the clay and silt

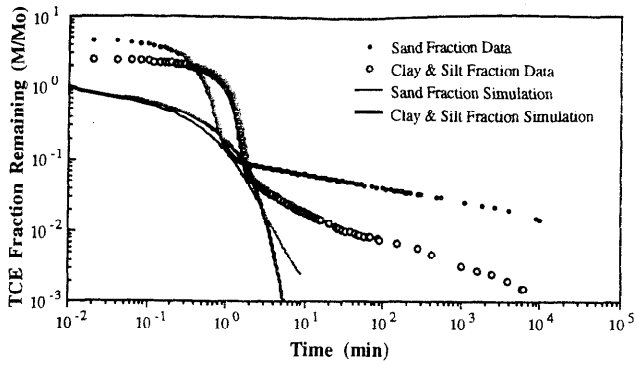

Figure 12. Comparison of simulations with experimental data for the sand and the clay and silt size fractions of the Livermore Aquifer solids.

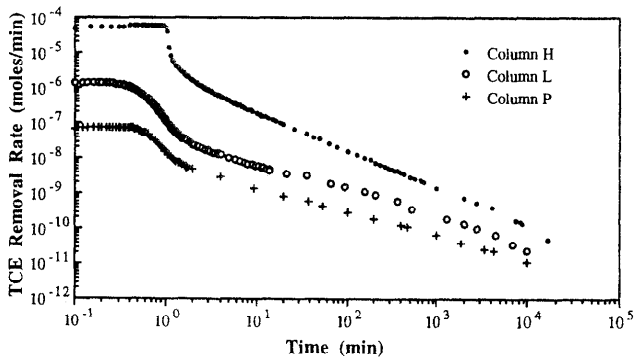

Figure 13. Comparison of TCE removal rates for three columns of the Santa Clara solids purged at ~17 mL/min with initial vapor concentrations of column H = 3.5 × 10^{-6} mol/mL; column L = 8.6 × 10^{-8} mol/mL; and pre-purged column P = 4.6 × 10^{-9} mol/mL.

fraction as compared to the sand fraction. Although the clay and silt isotherm is linear, greater sorption on the clay and silt fraction leads to a greater R_{int} for fractional removals less than 99%. Therefore, only for TCE removals >99% can differences in isotherm shape lead to faster desorption for the clay and silt fraction. Comparison of simulations for the sand and the clay and silt fractions in Figure 12 shows that only for $M/M_o < 0.01$ is the clay and silt fraction expected to have a shorter removal time than the sand fraction. The χ_e used on each fraction was that which best matched the time points for release of the fast desorbing TCE, i.e., 90% removal on the sand and 95% on the clay and silt. As with the silica gels, these model simulations fail to match the slow desorption of the last 5–10% of sorbed TCE.

Santa Clara Aquifer Solids. Experiments investigating the effect of initial concentration similar to those with the silica gel were performed on the Santa Clara solids. For columns H and L, the initial concentrations in Figure 13 were the highest concentrations to which these solids were exposed. Column P, however, was initially at the same concentration as column H, but was previously purged for 2 weeks and subsequently shut-in for 3 months prior to the purge shown in Figure 13. Differences in desorption behavior between columns H, L, and P are not immediately evident from Figure 13 where the removal rate profiles for all three columns are similar in shape. However, Figure 14 shows that column H has both fast and slow desorbing fractions, while column P has only slow desorbing TCE. In Figure 14, column P had both a lower initial sorbed concentration, and a lower initial vapor concentration than column L. However, after 10^4 min of purging, column P had 81% more TCE remaining than

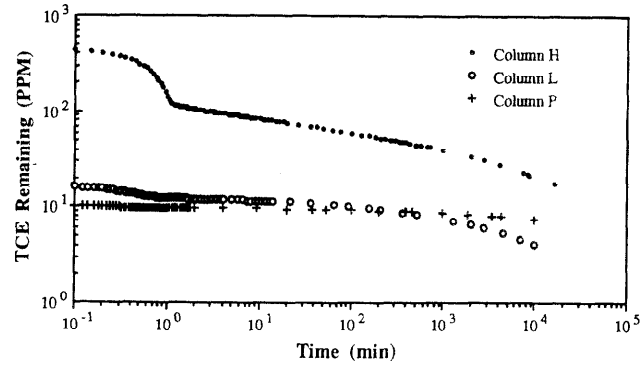

Figure 14. TCE remaining in three columns of the Santa Clara Aquifer solids with different initial concentrations for the removal rate data in Figure 13.

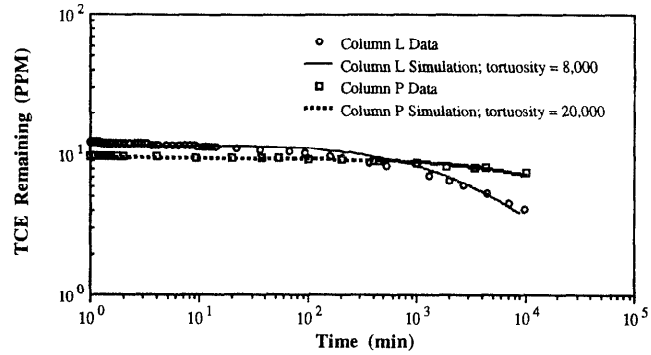

Figure 15. Comparison of data with model simulations for columns L and P of the Santa Clara Aquifer solids.

column L. The fractional TCE removal in Figure 14 is 96% from column H, 68% from column L, and 24% from column P.

Isotherm nonlinearity may account for some differences in TCE desorption rates between columns H, L, and P. However, the greater residual in column P compared to column L can only be explained by hysteresis. Figure 14 in the preceding paper (*14*) demonstrates hysteresis on the Santa Clara solids. In Figure 13, the initial solids concentration in column L is lower by a factor of 2 as compared to the desorption isotherm at that vapor concentration (8.6 × 10^{-8} mol/mL).

In Figure 15, a pore diffusion model simulation for Santa Clara column P is compared with experimental data, and a reasonable visual fit can be obtained with χ_e = 20 000. For Santa Clara column L, the data can be reasonably modeled with a χ_e = 8000. In light of the agreement between the pore diffusion model and the data in Figure 15, χ_e in the range of 8000–20 000 appears to be characteristic of the Santa Clara solids. However, Figure 16 shows that using a χ_e = 8000 in a model simulation for Santa Clara column H leads to greatly underestimating the rate of TCE removal. Also shown in Figure 16 is a simulation for column H using χ_e = 22. Since this simulation yields a similar time as the experimental data for fast site desorption (~65% TCE removal), this χ_e may be approximately representative of diffusion through the macro- and mesopores on the Santa Clara solids.

As with the other solids, the pore diffusion model is not capable of simulating both the fast and the slow desorbing fractions on the Santa Clara solids. Lower initial TCE concentrations lead to smaller fast desorbing fractions and better fits to the pore diffusion model if high χ_e are used. The pore diffusion model matches the column P data

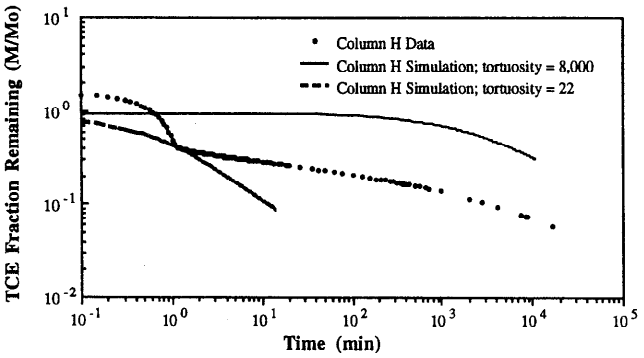

Figure 16. Comparison of experimental data with simulations using different effective tortuosity factors for Santa Clara column H.

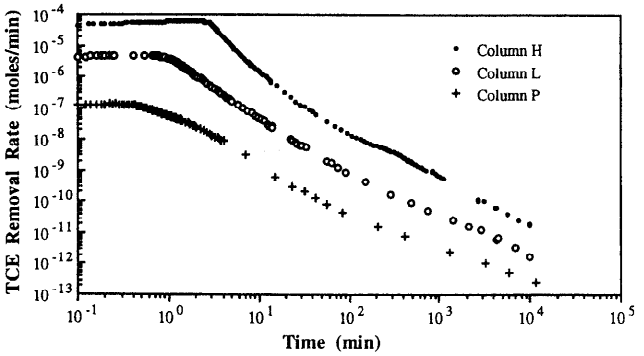

Figure 17. Comparison of TCE removal rates for three columns of Norwood soil purged at ~15 mL/min with initial vapor concentrations of column H = 3.3×10^{-6} mol/mL; column L = 3.0×10^{-7} mol/mL; and pre-purged column P = 7.7×10^{-9} mol/mL.

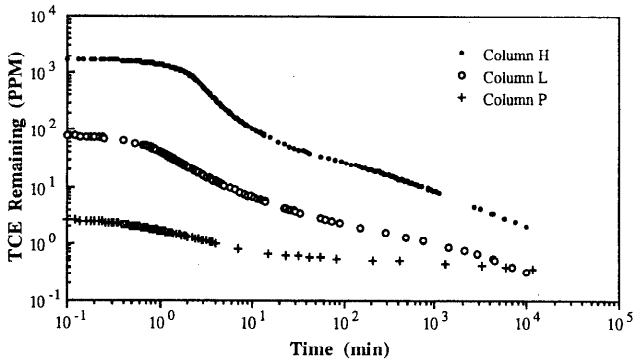

Figure 18. TCE remaining in three columns of Norwood soil with different initial concentrations for the removal rate data in Figure 17.

reasonably well because the fast desorbing fraction is small and nearly all TCE desorbs on a similar time scale. However, Figures 15 and 16 show that the χ_e best matching the data for columns H, L, and P is not constant, but is dependent on the initial concentration. This indicates that the pore diffusion model fails to mechanistically describe desorption and is, therefore, reduced to a non-mechanistic, single-fitting parameter model.

Norwood Soil. Desorption experiments with three initial concentrations similar to those performed with the silica and Santa Clara solids were performed on the Norwood soil. One difference was that the time between the first and second purgings of column P was increased to 6 months, compared to 3 months for both the silica and Santa Clara solids. The removal rate profiles for TCE from Norwood soil in Figure 17 are similar in shape for all three initial concentrations, but Figure 18 shows that TCE desorption behaves hysteretically. At the start of the purge, both the TCE vapor and solids concentrations in column L were higher than those in column P, but after purging, column L had less TCE remaining than column P. The initial column L distribution of TCE between the sorbed and vapor phases is characteristic of the adsorption branch of the TCE isotherm, while the column P distribution is representative of the desorption branch. In Figure 17, the initial sorbed concentration in column L was 40% less than the sorbed concentration on the desorption isotherm at that vapor concentration (cf. Figure 15 in ref 14).

Table 5. Freundlich Exponents for Adsorption from Solution and Times for Removal of 99% of Sorbed TCE in Experiments with Initial TCE Saturations of ~70% P/P_0

solid	$1/n$	99% removal time (days)
Livermore clay and silt	1.03	0.021
montmorillonite	0.97	0.014
Norwood	0.81	0.45
glass beads	0.75	17
silica gel D	0.71	1.4
silica gel B	0.64	9.0
silica gel A	0.61	17
silica gel C	0.55	16
Livermore sand	0.48	28
Santa Clara	0.38	56

Discussion

The methods used in this investigation allowed continuous measurement of desorption rates over more than 7 orders of magnitude. The finding that desorption proceeds on two distinct time scales is consistent with previous investigations (*4, 24–26*). At TCE concentrations near vapor saturation, the majority of TCE desorbs within 10 min, while removal of the remaining fraction requires weeks or months. The finding that the slowly released fraction increases with decreasing sorbate concentration is also consistent with other investigations (*4, 5*), and indicates preferential sorption in the slow sites. Preferential sorption implies a higher adsorption energy for these slow sites. However, high-energy sorption alone is unlikely to account for the slow release given that adsorption energies much greater than those for physical adsorption must be assumed to account for the greatly increased sorptive residence time. Physical adsorption energies are generally in the range of 2–10 kJ/mol, but an energy greater than 80 kJ/mol is required to increase the sorptive residence time above 1 min (*27*). This indicates that restricted transport must accompany higher energy sorption to account for the slow release.

Measurable solid properties including internal porosity, natural organic matter content, internal surface area, pore size, and particle size showed no correlation with the fraction of slow desorbing TCE. The only measurable parameter which correlates with the fraction of slowly released sorbate is the Freundlich isotherm exponent. Table 5 gives the measured times required for 99% TCE removal along with the Freundlich isotherm exponents for the high concentration experiments (TCE vapor saturations ~70%). There is a general inverse correlation between the Freundlich isotherm exponents and the time for 99% TCE desorption. However, increases in R_{int} due to isotherm nonlinearity are not sufficient to account for the slowly released fractions.

The kinetic and isotherm data implicate intragranular micropores of mineral solids as responsible for both

isotherm nonlinearity and the slowly released fraction. This conclusion contrasts with other investigations which implicate restricted diffusion through natural organic matter (*1, 19*) or mesopore diffusion (*6*) as responsible for the slow release of sorbed contaminants. Results from this research also indicate that the pore diffusion model, which treats all pores as a continuum, may not be applicable where micropore adsorption is significant.

Glossary

C_w	aqueous solute concentration (M/L^3)
D_a	aqueous diffusion coefficient (L^2/T)
D_e	effective diffusion coefficient (L^2/T)
ϵ_i	intraaggregate porosity (–)
K_d	solid/solution distribution coefficient (L^3/M)
K_F	Freundlich capacity coefficient ($(L^3/M)^{1/n}$)
K_r	restrictivity factor (–)
λ	the ratio of critical molecular diameter (*8*) to the pore diameter (–)
$1/n$	Freundlich isotherm exponent
P	vapor pressure
P_o	vapor saturation pressure
r	radial spatial coordinate (L)
r_a	particle radius (L)
ρ_g	grain density (mass of solid per total grain volume) (M_s/L^3)
t	time (T)
τ_d	dimensionless time scale for radial diffusion (–)
χ	tortuosity factor (–)
χ_ϵ	effective tortuosity (–)

Acknowledgments

This work was supported in part by the US EPA Office of Exploratory Research, Washington, DC, under Agreement R-815738-01 through the Western Region Hazardous Substance Research Center. Additional support was provided by Lawrence Livermore National Laboratories through B116830. Thanks go to Peter Grathwohl for his pore diffusion model, to C. J. Werth for his contributions to the characterization of the solids, and to George M. Deeley of Shell Development Co., Houston, TX, for providing us with the Norwood soil. The content of this paper does not necessarily represent the views of the supporting organizations.

Literature Cited

(1) Nkedi-Kizza, P. L.; Brusseau, M. L.; Rao, P. S. C.; Hornsby, A. G. *Environ. Sci. Technol.* **1989**, *23*, 814.
(2) Ball, W. P.; Roberts, P. V. *Environ. Sci. Technol.* **1991**, *25*, 1223.
(3) Grathwohl, P.; Gewald, T.; Pyka, W.; Schuth, C. In *Contaminated Soil '93*; Bosman, R., van den Brink, W. J., Eds.; Kluwer Academic: The Netherlands, 1993; pp 175–184.
(4) Pignatello, J. J. *Environ. Toxicol. Chem.* **1990**, *9*, 1107.
(5) Pignatello, J. J. *Environ. Sci. Technol.* **1990**, *9*, 1117.
(6) Wu, S.; Gschwend, P. M. *Environ. Sci. Technol.* **1986**, *20*, 717.
(7) Crank, J. *The Mathematics of Diffusion*, 2nd ed.; Clarendon Press: Oxford, 1975.
(8) Chantong, A.; F. E. Massoth. *AIChE J.* **1983**, *29*, 725.
(9) Satterfield, C. N.; Colton, C. K.; Pitcher, W. H. *AIChE J.* **1973**, *19*, 628.
(10) Wakao, N.; Smith, J. M. *Chem. Eng. Sci.* **1962**, *17*, 825.
(11) IUPAC. Manual of Symbols and Terminology. *Pure Appl. Chem.* **1972**, *31*, 578.
(12) Dubinin, M. M. In *Characterisation of Porous Solids*; Gregg, S. J., Sing, K. S. W., Eds.; Society of Chemical Industry: London, 1979.
(13) Kiselev, A. V. *Discuss. Faraday Soc.* **1971**, *52*, 14.
(14) Farrell, J.; Reinhard, M. *Environ. Sci. Technol.*, preceding paper in this issue.
(15) de Boer, J. H. *The Dynamical Character of Adsorption*; Clarendon Press: Oxford, 1968.
(16) Steinberg, S. M.; Pignatello, J. J.; Sawhney, B. L. *Environ. Sci. Technol.* **1987**, *21*, 1201.
(17) Farrell, J. Ph.D. Dissertation, Stanford University, 1993.
(18) Pignatello, J. J. In *Reactions and Movements of Organic Chemicals in Soils*; Soil Science Society of America: Madison, WI, 1989.
(19) Bouchard, D. C.; Wood, A. L.; Campbell, M. L.; Nkedi-Kizza, P.; Rao, P. S. C. *J. Contam. Hydrol.* **1988**, *2*, 209.
(20) Grathwohl, P.; Reinhard, M. *Environ. Sci. Technol.* **1993**, *27*, 2360.
(21) Unger, K. K. *Porous Silica*; Elsevier Scientific: New York, 1979.
(22) Parfitt, R. L.; Greenland, D. J. *Clay Miner.* **1970**, *8*, 305.
(23) Gregg, S. J.; Singh, K. S. W. *Adsorption, Surface Area, and Porosity*; Academic Press: New York, 1982.
(24) Karickhoff, S. W. *J. Hydraul. Eng.* **1984**, *110*, 707.
(25) Di Toro, D. M.; Horzempa, L. M. *Environ. Sci. Technol.* **1982**, *16*, 594.
(26) McCall, P. J.; Agin, G. L. *Environ. Toxicol. Chem.* **1985**, *4*, 37.
(27) Adamson, A. W. *Physical Chemistry of Surfaces*; Wiley Interscience: New York, 1982.

Received for review March 11, 1993. Revised manuscript received September 21, 1993. Accepted October 4, 1993.[⊗]

[⊗] Abstract published in *Advance ACS Abstracts,* November 15, 1993.